RSC Advances

PAPER

View Article Online
View Journal | View Issue



Cite this: *RSC Adv.*, 2023, **13**, 33595

# Influence of surface structure on friction and wear characteristics of silicone rubber for hydraulic rod seals

Sung-Jun Lee and Chang-Lae Kim *

This research investigates the impact of surface structure on the friction and wear characteristics of silicone rubber used as a material for hydraulic rod seals. Various silicone rubber specimens with different surface structures were prepared, and their surface morphology, water contact angle, and surface roughness were compared. Friction tests were conducted using a reciprocating sliding method to evaluate the friction coefficient and wear characteristics. The results revealed that the silicone rubber specimens coated with silicone powder exhibited a significant increase in surface roughness. However, this increase was accompanied by a decrease in surface energy, leading to the absorption and dispersion of contact pressure and frictional stress, resulting in a friction-reducing effect. Consequently, the silicone rubber specimens coated with silicone powder demonstrated a friction coefficient more than 70% lower on average compared to bare silicone rubber, and exhibited minimal wear characteristics. The irregular microstructures formed on the surface of the silicone rubber are believed to contribute to these friction and wear improvements. Alterations in stress and contact behavior of bare silicone rubber and silicone powder-coated silicone rubber with pre-curing time during indentation and sliding movements were validated through finite element analysis. These findings provide valuable insights for enhancing the performance and durability of hydraulic rod seals made from silicone rubber. This research is expected to contribute to further studies aimed at improving hydraulic seal materials.

Received 23rd September 2023
Accepted 12th November 2023

DOI: 10.1039/d3ra06485a

rsc.li/rsc-advances



## 1. Introduction

Hydraulic rod seals are components used to prevent leakage and contamination of hydraulic fluid in reciprocating motion devices. Hydraulic rod seals operate during both the out-stroke and in-stroke, meaning that the friction surfaces are almost in contact, and friction occurs due to the presence of lubricant or contact surfaces. Therefore, the surface roughness of the contacting rod seal significantly influences its dynamic friction behavior, directly affecting lubricant film formation and rupture at the interface.[1] Consequently, numerous studies have been conducted to investigate the influence of surface roughness on lubrication mechanisms and friction characteristics of rod seals.[2–5]

Feng *et al.* reported that the surface roughness of the counter material, a stainless steel plate, significantly affects the friction and wear behavior of elastomers when the rubber cylinder slides on the rough surface under lubricated conditions.[6] Scaraggi *et al.* proposed a multiscale mean field model using the average field theory to analyze the effect of anisotropic surface roughness on rod seal friction.[7] He *et al.* fabricated silicone rubber samples with various surface structures and conducted friction tests to investigate the effect of surface structures on friction.[8] The friction coefficient of silicone rubber with applied surface structures was found to be significantly lower than that of smooth surfaces, based on the results of friction tests performed under various loads. Ryu *et al.* produced silicone rubber with microstructures inspired by lotus leaf structures.[9] The successful replication of microstructures in the silicone rubber demonstrated the formation of microstructures exhibiting superhydrophobicity. Furthermore, wear tests were conducted to evaluate the friction and wear characteristics of the microstructures, and the results confirmed the improvement of friction and wear properties compared to smooth surfaces.

Numerous studies have been conducted to investigate the influence of surface structures on the friction and wear properties of silicone rubber. However, existing processes mainly utilize replicated surfaces from molds, which present difficulties in mass production and raise concerns regarding stress concentration and damage upon demolding. Additionally, most studies have been performed on plate-shaped samples, which pose challenges in creating three-dimensional structures or fabricating them into actual components.

Therefore, it is necessary to conduct research on a process that can produce stable structures, including friction and wear characteristics, that is simple in fabrication, allows for mass

*Department of Mechanical Engineering, Chosun University, Gwangju, 61452, Republic of Korea. E-mail: kimcl@chosun.ac.kr*

production, and enables the production of actual components. This research should also encompass durability studies.

Silicone rubber, employed as a material for rod seals, has exhibited versatile applications across various domains including engineering, optics, and electronics due to its remarkable attributes such as excellent heat resistance, chemical resilience, and elasticity.[10] However, elastomeric materials like silicone rubber display elevated levels of friction and wear when sliding against surfaces of relatively higher strength.[11,12] Overcoming these limitations necessitates an investigation into the mechanisms taking place within the contact region of the silicone rubber surface. Therefore, a comprehensive exploration is imperative to mitigate silicone rubber friction in the context of the frictional phenomena occurring between two contacting materials.

In the case of dry sliding friction, the friction and wear characteristics of silicone rubber deviate from those of conventional metallic materials, showing dependence on diverse intrinsic and extrinsic parameters, alongside mechanical properties.[13,14] Influential factors impacting silicone rubber friction encompass stiffness, surface roughness, sliding speed, and contact area.[15–17] The mechanical strength of silicone rubber significantly influences the contact area, while the utilization of lubricants serves to mitigate the frictional interaction between the rubber and the substrate.[18]

Johnson *et al.* conducted an extensive investigation into the friction and wear mechanisms of silicone rubber.[19] As per experimental findings, a 10 : 1 silicone rubber ratio exhibited micro-plowing wear under low loads, while cutting wear manifested under high loads. Conversely, a softer 20 : 1 silicone rubber ratio demonstrated more uniform wear, showcasing elasticity as a fusion of fatigue-based wear and abrasive wear. Addressing the friction and wear challenges of silicone rubber, strategies such as incorporation of high-strength nanoparticle fillers or microstructuring have been proposed.[20,21] However, the incorporation of fillers enhances the mechanical strength of silicone rubber, yet it results in a reduction of the material's inherent elasticity. Furthermore, microstructuring necessitates sophisticated techniques involving photoresists and laser/etching for mold creation, with potential risks of mold and rubber separation damage during the process.

This study endeavors to introduce an efficacious approach to mitigate friction while preserving the strength of silicone rubber through a straightforward fabrication process. To attain this goal, we scrutinize the impact of surface structure on the friction and wear characteristics of silicone rubber. The effect of diverse surface microstructures on the friction and wear behavior of silicone rubber is investigated by assessing their friction and wear characteristics and analyzing the stress behavior through finite element analysis.

# 2. Materials and methods

## 2.1 Specimen fabrication

In this study, various silicone rubber specimens with different surface structures were prepared to evaluate their friction and wear characteristics. To produce stable powders with a uniform distribution of heat throughout the silicone rubber, a sugar templating process was employed by introducing a porous structure into the silicone rubber. Fig. 1 shows the specimen fabrication process. Silicone rubber (Sylgard 184, Dow High Tech, Goyang, Korea) base and curing agent were mixed at a 10 : 1 ratio and then poured into a Petri dish containing cubic sugar. The mixture was degassed in a vacuum chamber for 30 minutes and cured for 2 hours in a 70 °C hot air oven. Subsequently, the silicone rubber surface was polished using sandpaper, and the cubic sugar was removed by immersion in boiling water and subsequent complete air-drying. Finally, the silicone rubber was subjected to heating at 350 °C in a furnace for 6 hours and subsequently cooled to 20–25 °C, resulting in the production of powdered silicone rubber. The silicone rubber base and curing agent were mixed in a ratio of 10 : 1 wt%, and before complete curing, the Petri dish containing the gel-like silicone rubber was inverted and placed into a beaker containing silicone powder. The pre-curing time of the silicone rubber was 5 minutes, 10 minutes, 20 minutes, 30 minutes, and 40 minutes, respectively. The specimens were then stored in an oven heated to 70 °C for 2 hours to ensure complete curing. After removing the remaining silicone particles on the specimen surface, they were separated from the Petri dish. Subsequently, they were soaked in ethanol, ultrasonically cleaned, and dried in an oven to obtain silicone rubber specimens with various surface structures. For comparison, pure silicone rubber specimens without silicone powder coating were also prepared. As can be seen in Table 1, in this study, the silicone rubber specimens are denoted as Bare silicone rubber (Bare SR), and the silicone rubber specimens coated with silicone powder according to pre-curing time are denoted as SP/SR-*x*. Here, *x* represents the pre-curing time.

## 2.2 Experiments

To analyze the changes in surface properties of silicone rubbers coated with silicone powders according to the surface structure, surface morphology was observed, and the contact angle of water droplets and surface roughness were measured. The contact angle was measured by dropping 10 μL of deionized water on the specimen surface and then using a microscope camera to measure the angle formed by the water droplet on the surface. Surface roughness was measured by contacting the

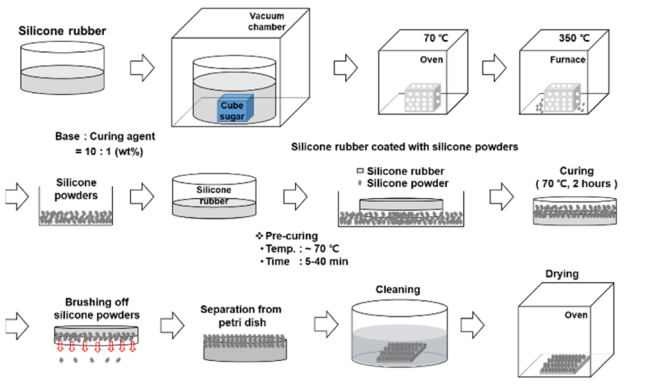


Fig. 1 Fabrication process of silicone powder-coated silicone rubbers.

Table 1 Fabrication conditions and names of various silicone rubber specimens

| | Materials | | |
|---|---|---|---|
| Specimen name | Silicone rubber | Silicone powder | Pre-curing time (min) |
| Bare SR | Silicone rubber base : curing agent (10 : 1 wt%) | — | — |
| SP/SR-PC5M | | Diameter: ~50 μm | 5 |
| SP/SR-PC10M | | | 10 |
| SP/SR-PC20M | | | 20 |
| SP/SR-PC30M | | | 30 |
| SP/SR-PC40M | | | 40 |

stylus tip with the specimen surface under a load of 0.75 mN and scanning in a straight line direction (SV-2100M4, Mitutoyo Korea Corporation, Gunpo, Korea). The centerline average roughness ($R_a$) value was obtained after scanning a 2 mm evaluation length.

To evaluate the friction and wear characteristics of silicone rubbers coated with silicone powders according to the surface structure, reciprocating motion friction tests were performed (RFW 160, NEOPLUS, Co., Ltd, Daejeon, Korea). The friction test conditions for the silicone rubber are summarized in Table 2. After applying a load of 20 mN by contacting a steel ball with a diameter of 1 mm to the specimen, a sliding friction test was performed. The experiment was conducted for a total of 2000 cycles at a sliding distance of 2 mm at a speed of 8 mm $s^{-1}$. The friction tests were conducted in an environment with a temperature of 25 °C and a humidity of 40%. In order to ensure the reliability of the experimental results, the tests were repeated three or more times, and the average values of the experimental results were utilized. After the experiment, wear tracks formed on the surfaces of the specimens were analyzed using an optical microscope.

## 3. Results and discussion

The surfaces of the silicone rubber specimens formed using the powder coating method were observed under the optical microscope, as shown in Fig. 2. The bare silicone rubber exhibited a very smooth surface morphology, whereas the silicone rubber specimens coated with silicone powders showed a highly rough surface morphology. On the surfaces of the silicon rubbers coated with silicon powders, silicon powders with a size of approximately 50 μm were embedded on the entire surfaces to form irregular surface morphologies.

The changes in surface properties of the specimens according to the surface structure were analyzed by measuring the water droplet contact angle and surface roughness. Fig. 3 shows the surface roughness of each specimen. The surface roughness of Bare SR was measured to be 0.24 μm, whereas the silicone powder-coated specimens, namely silicone powders coated silicone rubber with precuring time 5 min (SP/SR-PC5M), silicone powders coated silicone rubber with precuring time 10 min (SP/SR-PC10M), silicone powders coated silicone rubber with precuring time 20 min (SP/SR-PC20M), silicone powders coated silicone rubber with precuring time 30 min (SP/SR-PC30M), and silicone powders coated silicone rubber with precuring time 40 min (SP/SR-PC40M), exhibited average surface roughness values of 3.2 μm, 3.17 μm, 3.17 μm, 3.33 μm, and 3.27 μm, respectively. Among these, Bare SR showed the lowest surface roughness, while the SP/SR-PC30M specimen, which was coated with silicone powder after 30 minutes of precuring, demonstrated the highest recorded surface roughness. Thus, the coating of silicone powder resulted in an increase in

Table 2 Tribo-test conditions

| Reciprocating type tribo-test | |
|---|---|
| Tip material | Steel ball ($D$: 1 mm) |
| Normal load | 20 mN |
| Sliding speed | 8 mm $s^{-1}$ |
| Sliding stroke | 2 mm |
| Sliding cycle | 2000 cycles |

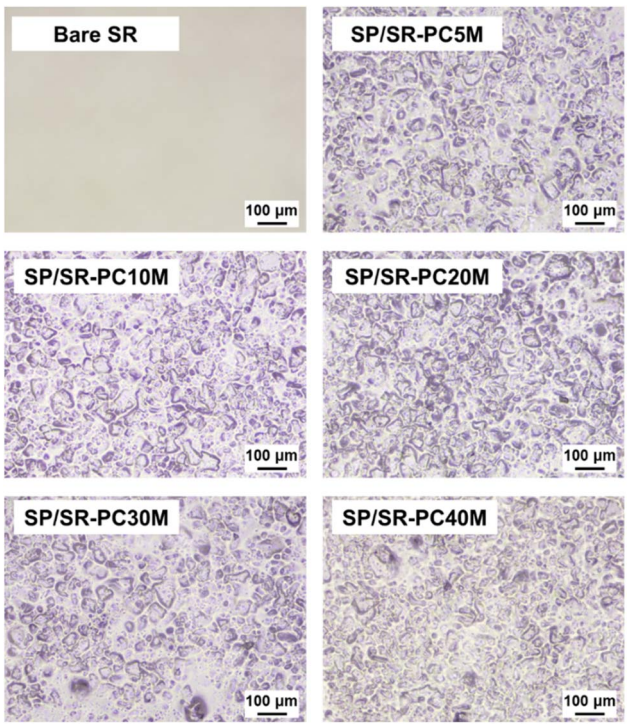


Fig. 2 Optical microscope images of bare silicone rubber and silicone powder-coated silicone rubbers according to the pre-curing time.

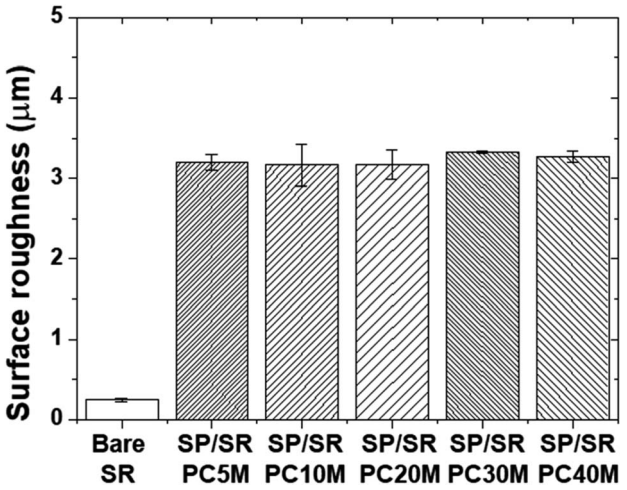


Fig. 3 Surface roughness of bare silicone rubber and silicone powder-coated silicone rubbers according to the pre-curing time.

the surface roughness of the silicone rubber. The combination of silicone powder and silicone rubber led to the formation of irregular microstructures on the surface, which contributed to the observed increase in surface roughness.

The contact angles of all the samples are depicted in Fig. 4. The contact angle of Bare SR measured 105°, while the contact angle of the silicone powder-coated silicone rubber ranged between 116° and 124°. Notably, the water droplet contact angle displayed higher values for the SP/SR-PC specimens that were coated with silicone powder in comparison to Bare SR. Moreover, an increase in the pre-curing time of the silicone rubber tended to lead to an increase in the contact angle. Silicone rubber comprises repetitive units of –O–Si$(CH_3)_2$– linked by covalent bonds between silicon (Si) and oxygen (O).[22] This molecular structure grants silicone rubber its hydrophobic attributes, primarily due to the hydrocarbon-forming methyl groups and alkyl portions adjacent to silicon atoms.[23] The presence of oxygen atoms in the silicone rubber structure facilitates cross-linking with silicon atoms along the main chain. These oxygen atoms, unconnected with methyl groups, contribute to maintaining the hydrophobic nature of silicone rubber.[24] The SP/SR-PC specimens, featuring microstructures resulting from the silicone powder coating, exhibit heightened hydrophobicity in silicone rubber as the alkyl portion density increases. This phenomenon can be attributed to the augmented presence of methyl groups, reinforcing the hydrophobicity of the polymer coating's surface. Furthermore, the introduction of microstructures onto the surface generates additional space, contributing to the anti-wetting properties resulting from the hierarchical structure and inherent hydrophobicity of silicone rubber itself.[25] Silicone rubber exhibits hydrophobicity, resulting in relatively large contact angles when in contact with water, owing to its low affinity for the interfacial region. As a result, hydrophobicity was observed for all specimens based on the contact angle measurements, and higher contact angles were observed for the SP/SR-PC specimens characterized by microstructures resulting from silicone powder coating. The introduction of microstructures into the silicone rubber leads to an increase in the contact angle due to the irregular surface structure. Therefore, the higher contact angles observed in the SP/SR-PC specimens with microstructures, compared to the smooth Bare SR, can be attributed to the formation of microstructures. Additionally, it is inferred that as the pre-curing time of the silicone rubber increases, the silicone powder coating layer is formed on the surface, resulting in higher contact angles.

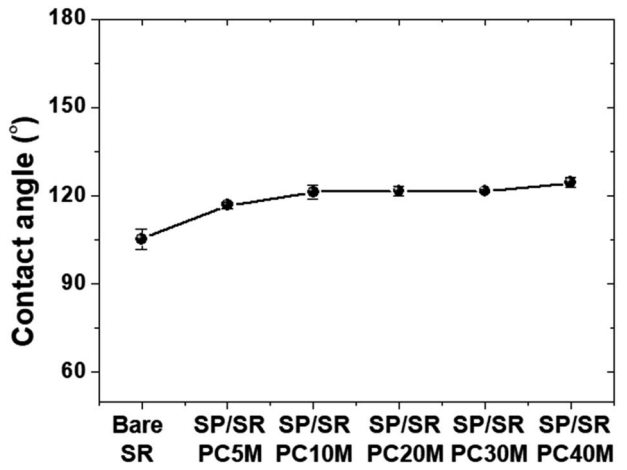


Fig. 4 Contact angles of silicone rubbers according to surface structure.

A reciprocating sliding friction test was performed on six different specimens with varying surface structures, and the changes in friction coefficients were compared as shown in Fig. 5(a). For the bare silicone rubber, the friction coefficient started at approximately 2.1 and increased to approximately 2.3 after 250 cycles. It then slightly decreased and remained relatively constant at approximately 2.25 until reaching 2000 cycles. In contrast, the silicone rubber specimens coated with silicone powders started with friction coefficients of approximately 0.6–0.7 in the initial cycles and showed minimal variation, maintaining relatively constant values until 2000 cycles were reached. As shown in Fig. 5(b), the average friction coefficients of the bare silicone rubber and the silicone rubber specimens coated with silicone powders were measured to be 2.29 and 0.62–0.74, respectively. The average friction coefficients of the silicone rubber specimens coated with silicone powders was more than 70% lower than that of the bare silicone rubber. The difference in friction coefficients among the silicone rubber specimens coated with silicone powders was very slight with respect to the pre-curing time. Notably, after 20 minutes of pre-curing, the specimen coated with silicone powders exhibited the lowest friction coefficient of 0.6.

During the reciprocating sliding motion involving the contact between silicone rubber and the steel ball, a substantial discrepancy in mechanical strength exists between the two materials, resulting in a notable expansion of the contact area between their respective surfaces.[26] Additionally, the intrinsic adhesion properties of silicone contribute to relatively heightened friction forces.[27] Ultimately, when complete contact occurs

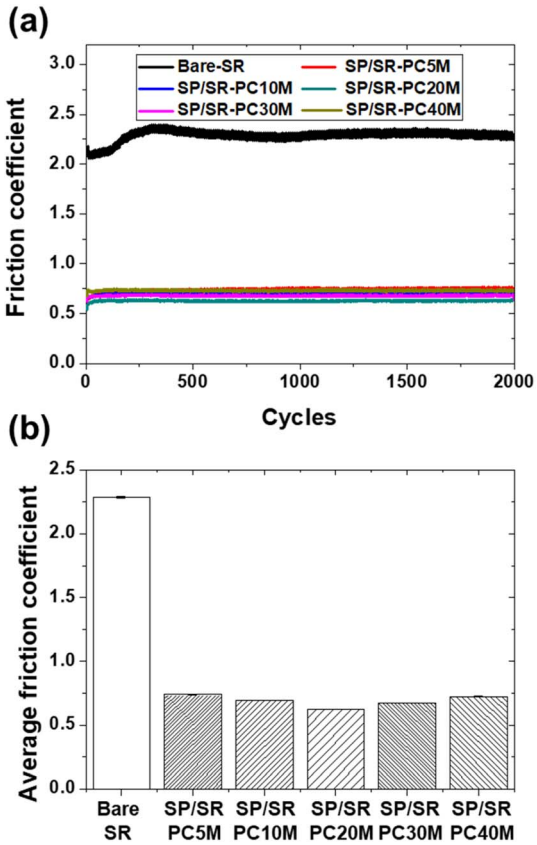


Fig. 5 Friction characteristics of bare silicone rubber and silicone powder-coated silicone rubbers according to the pre-curing time: (a) friction coefficient history and (b) average friction coefficient.

between two surfaces, frictional force increases in this region. Particularly under dry conditions, during reciprocating axial sliding motion, deformation transpires at the contact interface. A force is applied to return this deformed structure to its initial state, ultimately resulting in the generation of additional friction through these physical reactions.[28] Furthermore, compressed silicone rubber lacks the capacity to promptly adjust to the sliding speed during recovery, leading to elevated friction forces. The material's limited adaptability during the compression-recovery process contributes to enhanced interaction and adhesion between the materials, thus resulting in escalated friction forces. Consequently, smooth-surfaced silicone rubber demonstrates increased resistance to sliding motion due to its innate adhesive attributes and modest mechanical strength. These attributes prompt a notable degree of indentation when interacting with the steel ball, effectively enlarging the contact area between the two materials. However, with the introduction of microstructures onto the surface of silicone rubber, there is a reduction in surface energy and subsequent diminution of adhesion force, which in turn comparatively diminishes the friction force.[9] Irregular microstructures formed by silicon powders embedded on the surface of silicone rubber act as a spring-like buffer to absorb and disperse contact pressure and frictional stress with the counter tip, resulting in lower frictional properties compared to smooth bare silicone rubber without microstructures.[8] Moreover, the microstructures formed by the silicone powders reduced the contact area and surface energy with the counter tip, leading to friction reduction effects. Additionally, microstructures distribute contact pressure evenly, reducing adhesive force and resulting in smoother frictional behavior while maintaining volume compression stability. This leads to a decrease in mechanical friction force compared to a smooth surface, ultimately showcasing characteristics of low friction.[29]

In other words, the friction behavior of SP/SR can exhibit low-friction characteristics due to the introduction of surface structures. The microstructures on the surface can reduce the contact area with relative materials, preventing an increase in friction force due to compression of silicone rubber. The contact area between SP/SR and relative materials can be altered by various factors such as surface structure, particle size of silicone powder, and bonding strength. In this study, we created irregular structures by controlling the degree of curing for silicone rubber which could maximize buffering effects. Consequently, the friction force of silicone rubber is influenced by its surface structure.

As shown in Fig. 6, the comparison of the wear tracks formed on the specimen surfaces revealed distinct differences. During repetitive sliding motion, the bare silicone rubber exhibited rough wear traces across the entire wear track. In contrast, the silicone rubber specimens coated with silicone powders showed significantly reduced wear and only partial detachment of the wear track. Similar to the observations in the friction

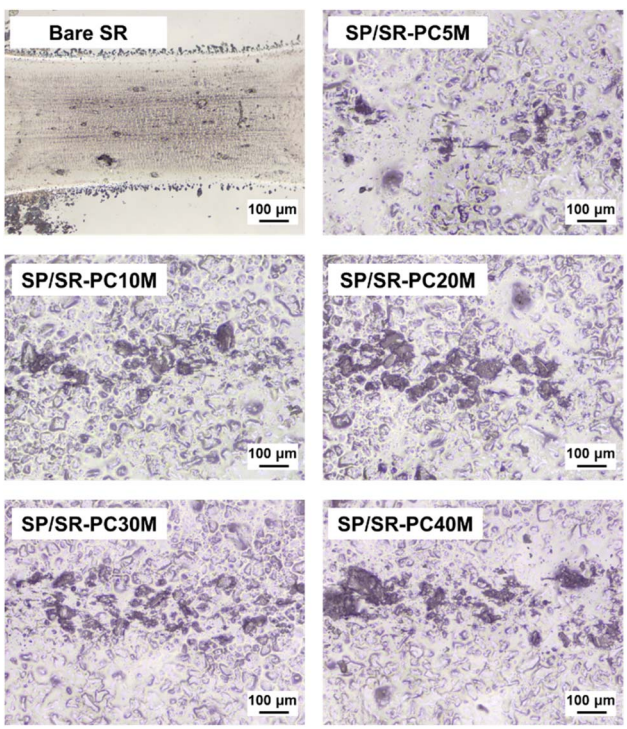


Fig. 6 Optical microscope images of wear tracks formed on the surfaces of bare silicone rubber and silicone powder-coated silicone rubbers according to the pre-curing time.

characteristics, the microstructures formed by the embedded silicone powder on the surface acted to absorb and disperse contact pressure and friction stress, resulting in minimal wear.[30–33] The specimens with shorter pre-curing times displayed relatively less wear traces. Accordingly, the silicone rubber with microstructures formed on the surface exhibited decreased surface energy and excellent friction and wear characteristics, owing to the absorption and dispersion of contact pressure and friction stress.

Fig. 7 shows the results of the finite element analysis to compare the internal stress behavior during indentation and contact sliding for Bare SR and SP/SR-PC. The evaluated Bare SR and SP/SR-PC specimens possessed dimensions of 1 mm in length and 0.1 mm in thickness. The elastic modulus of silicone rubber was obtained from previous research, and the friction coefficient was obtained from the results of this study.[34] The identical 1 mm diameter steel ball employed in the friction test served as the model for the counter material. The elastic modulus of the steel ball was 210 GPa with a Poisson's ratio of 0.35, whereas the silicone rubber exhibited an elastic modulus of 2 MPa and a Poisson's ratio of 0.5. The simulation analysis conditions entailed applying a 20 mN load to a fixed specimen in conjunction with a counter tip, succeeded by a 0.5 mm stroke. Considering the deformation of the silicone rubber, a dense mesh was formed in the contact area. As shown in Fig. 8, the contact pressure, von Mises stresses, and frictional shear stresses of Bare SR and SP/SR-PC presented different trends. Both specimens experienced the highest stresses on the surfaces in contact with the counter materials, with the stress being propagated around the contact points. This outcome serves to validate that stress is dispersed due to the viscoelastic characteristics of silicone rubber.[35] In indentation, the contact pressure within the contact area demonstrated a propensity to be proportionate to the specimen's mechanical properties, as evidenced in Fig. 8(a), where an increase in steel ball indentation depth corresponded to heightened contact pressure. Bare SR exhibited maximum indentation depths of 7 μm and contact pressure of 0.2 MPa under a 20 mN load, while SP/SR-PC displayed an indentation depth of 8 μm and a contact pressure of 0.56 MPa. It is posited that the smaller contact area of the SP/SR-PC specimen, owing to its surface structure, culminated in localized pressure on this structure's surface. However, the distributed stresses around the central point were less extensive. Fig. 8(b) and (c) show the stress variations during the sliding process. The sliding motion exhibited significant differences in stress generation within the silicone rubber's surface and interior. While Bare SR maintained constant stress without significant fluctuations, the SP/SR-PC specimen underwent cyclically alternating stress increments and decrements, forming a sinusoidal pattern. Additionally, the smooth-surfaced Bare SR encountered stress applied across its entire contact surface with the counter tip, with the stress distributed throughout its interior during sliding. In contrast, SP/SR-PC with microstructures exhibited relatively elevated stress levels on the surface in contact with the counter tip, and the internal stress propagation was comparatively restrained. Conversely, the trend of frictional shear stress differed. Bare SR maintained a consistent pressure of 0.3 MPa throughout the 0.5 mm sliding process, while SP/SR-PC manifested repeated stress oscillations, with a maximum stress value falling below 0.3 MPa, thereby indicating lower stress levels than Bare SR. Consequently, the stress and contact pressure on the silicone rubber surface were found to be higher in SP/SR-PC, a result of the microstructures formed by the silicone powders coated on the silicone rubber surface, which impede stress transfer beneath the silicone rubber surface by directly absorbing contact stress. The maximum stress value in SP/SR-PC was observed on the surface, indicating that the internal stress distribution within the

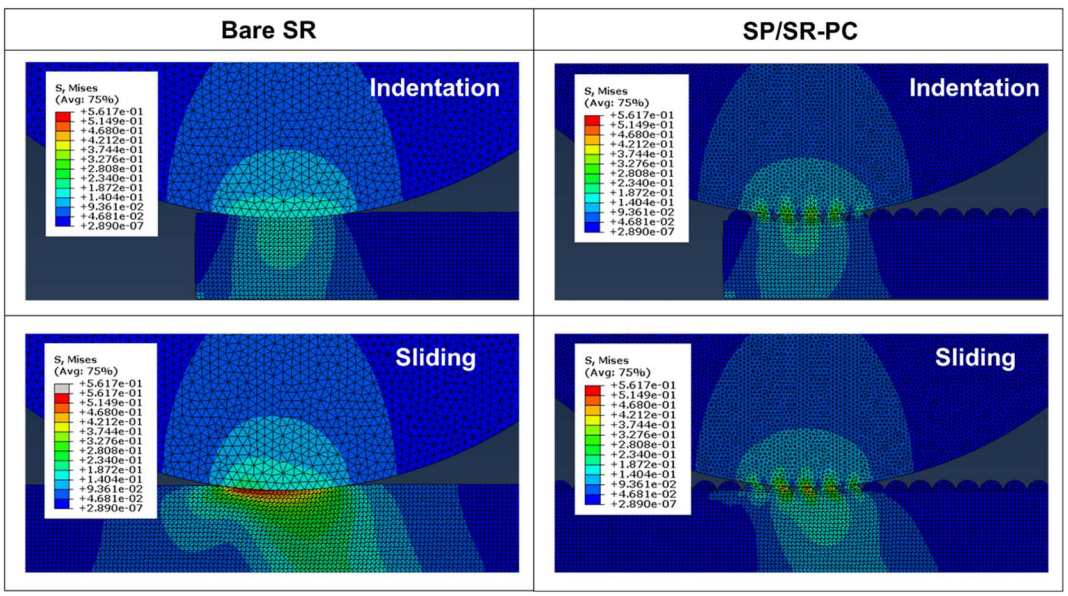


Fig. 7 FEA simulation results for bare silicone rubber and silicone powder-coated silicone rubber during indentation and contact sliding.

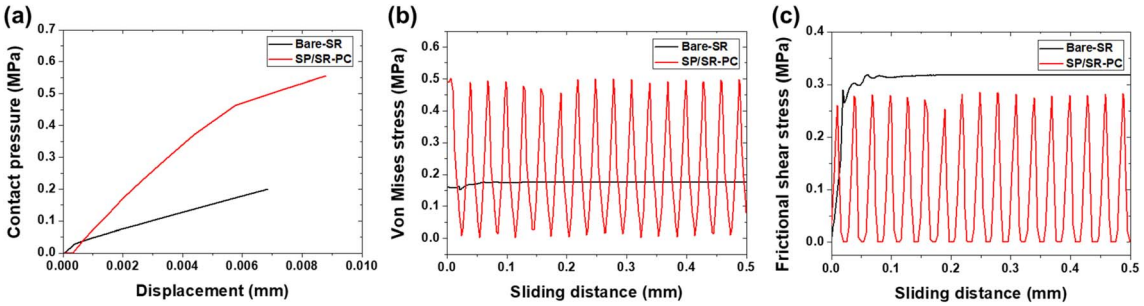


Fig. 8 Stress behavior analysis: (a) contact pressure, (b) von Mises stress and (c) frictional shear stress of bare silicone rubber and silicone powder-coated silicone rubber.

silicone rubber is less pronounced than that in Bare SR. The divergence in stress between the specimen's surface and interior due to external forces is anticipated to significantly influence the wear resistance of silicone rubber. Therefore, these findings substantiate that silicone rubber with formed microstructures exhibits superior low-friction characteristics in comparison to smooth-surfaced silicone rubber and displays wear resistance capable of withstanding contact without surface impairment.

Fig. 9 depicts a schematic representation of the wear mechanism during sliding motion for both Bare SR and SP/SR-PC. In the case of Bare SR, the surface experiences compression and comes into contact with the entire counter tip surface due to the mechanical strength and applied normal load.[29] This phenomenon is typically observed in elastomeric materials. Consequently, the contact area expands, and as the sliding motion advances, the counter tip becomes entangled with the specimen surface, leading to an escalation in frictional resistance. As a consequence, Bare SR exhibits the highest friction coefficient. With repeated sliding motions, adhesion and deformation arise from compression and recovery between the counter tip and Bare SR, eventually resulting in wear on the comparatively less robust surface of silicone rubber.[28] Hence, adhesive and fatigue wear mechanisms occur simultaneously, generating wear debris that adheres to the silicone rubber surface, rendering it considerably rough.[19] In contrast, during the initial contact phase of SP/SR-PC, deformation transpires on the microstructured surface as it encounters the counter tip. Furthermore, the coated silicone powders have low mechanical strength, causing the microstructured surface to engage evenly with the counter tip throughout the contact process. However, only the structural segment formed by the silicon particles embedded in the silicone rubber surface undergoes compression upon contact with the counter tip.[9] As a result, there is relatively limited contact between the counter tip and the silicone rubber surface, which typically leads to significant friction. The primary interaction takes place with the silicone powders, reducing the contact area and consequently lowering the frictional resistance during the sliding motion. Additionally, the microstructures on the surface experience less wear due to the localized stress acting on the surface and a cushioning effect during sliding compared to a smooth surface. Therefore, under identical friction test conditions, the friction coefficient of SP/SR-PC was significantly lower than that of Bare SR. Nonetheless, the silicone powders embedded in the SP/SR-PC surface experience delamination from the surface due to prolonged sliding friction. This outcome is likely due to the recurring contact pressure weakening the bond between the silicone rubber and the silicone powders, resulting in partial surface wear and eventual detachment of the silicone powders. The areas where the silicone powders delaminate manifest relatively substantial damage. This wear phenomenon varies according to the curing time of the silicone rubber. A shorter curing time results in silicone rubber being closer to a liquid state, thereby fostering extended bonding with the silicone powders and the formation of a stable surface.[12] Conversely, with an increase in curing time, the silicone rubber undergoes hardening, leading to diminished bonding on the surface, which in turn contributes to more pronounced wear. In summary, the wear of SP/SR-PC is postulated to be notably influenced by the bonding force between the silicone rubber and the silicone powders.

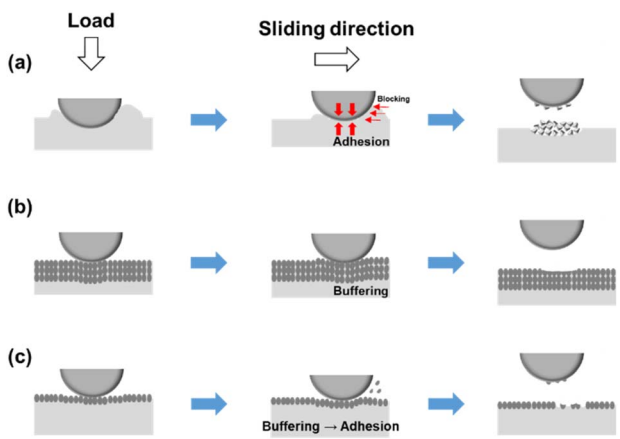


Fig. 9 Schematic designs of wear mechanisms of (a) bare silicone rubber and (b and c) silicone powder-coated silicone rubbers: (b) short curing time and (c) long curing time.

## 4. Conclusions

In this study, the influence of surface structures on the friction and wear characteristics of silicone rubber, which is the

material used for hydraulic rod seals, was analyzed. Specimens with different irregular microstructures were prepared by varying the pre-curing time during the silicone rubber curing process and coating them with silicone powders. The surface properties, including surface morphology, water droplet contact angle, and surface roughness of the specimens, were compared. Through reciprocal sliding friction tests, it was found that the silicone rubbers coated with silicone powders exhibited a significant reduction of over 70% in friction coefficient compared to the bare silicone rubber, along with relatively minor wear traces. The reason for the reduced friction coefficient and wear in silicone rubber coated with silicone powders appears to be related to the microstructures formed by the embedded silicone powders. Specifically, the irregular microstructures formed by the silicone powders on the surfaces of the silicone rubbers led to a substantial increase in surface roughness, while simultaneously reducing surface energy, resulting in friction reduction. The contact sliding behavior of Bare SR and SP/SR-PC was analyzed using FEA simulation, and the analysis revealed distinct stress behavior between the two specimens. The absorption and dispersion effects of contact pressure and friction stress due to these microstructures contributed to the improvement of friction and wear characteristics. The findings of this study are expected to contribute to the enhancement of the performance and durability of hydraulic rod seal materials.

## Author contributions

Sung-Jun Lee: conceptualization, methodology, software, validation, formal analysis, investigation, data curation, writing – original Draft, writing – review & editing, visualization. Chang-Lae Kim: conceptualization, methodology, resources, writing – review & editing, supervision, project administration.

## Conflicts of interest

There are no conflicts to declare.

## Acknowledgements

This results was supported by “Regional Innovation Strategy (RIS)” through the National Research Foundation of Korea (NRF) funded by the Ministry of Education (MOE) (2021RIS-002).

## References

1 S. Thielen, P. Breuninger, H. Hotz, C. Burkhart, T. Schollmayer, B. Sauer, S. Antonyuk, B. Kirsch and J. C. Aurich, *Tribol. Int.*, 2021, **155**, 106764.
2 B. Wang, X. Meng, X. Peng and Y. Chen, *Tribol. Int.*, 2021, **156**, 106791.
3 S. Bhaumik, A. Kumaraswamy, S. Guruprasad and P. Bhandari, *Tribol. Ind.*, 2015, **37**, 264.
4 S. Li, S. Xiu, W. Song, C. Sun and H. Yang, *Smart Mater. Struct.*, 2022, **31**, 075021.
5 W. Zhao, G. Zhang and G. Dong, *Friction*, 2021, **9**, 697–709.
6 D. Feng, M.-x. Shen, X.-d. Peng and X.-k. Meng, *Tribol. Lett.*, 2017, **65**, 1–14.
7 M. Scaraggi, J. Angerhausen, L. Dorogin, H. Murrenhoff and B. Persson, *Wear*, 2018, **410**, 43–62.
8 B. He, W. Chen and Q. Jane Wang, *Tribol. Lett.*, 2008, **31**, 187–197.
9 B.-H. Ryu and D.-E. Kim, *CIRP Ann.*, 2015, **64**, 519–522.
10 Q. Zhu, Z. Wang, H. Zeng, T. Yang and X. Wang, *Composites, Part A*, 2021, **142**, 106240.
11 S.-J. Lee, G.-M. Kim and C.-L. Kim, *Coatings*, 2021, **11**, 603.
12 S.-J. Lee and C.-L. Kim, *Polym. Test.*, 2023, **122**, 108018.
13 S.-J. Lee, G.-M. Kim and C.-L. Kim, *J. Mech. Sci. Technol.*, 2022, **36**, 1997–2005.
14 S.-J. Lee, Y.-C. Sohn and C.-L. Kim, *Materials*, 2022, **15**, 3262.
15 S. B. Iyer, A. Dube, N. Dube, P. Roy and R. Sailaja, *J. Mech. Behav. Biomed. Mater.*, 2018, **86**, 23–32.
16 I. Penskiy, A. Gerratt and S. Bergbreiter, *J. Micromech. Microeng.*, 2011, **21**, 105013.
17 H. Gatzen and M. Beck, *Wear*, 2003, **254**, 907–910.
18 S.-J. Lee, A. Amanov and C.-L. Kim, *J. Mech. Sci. Technol.*, 2023, 1–9.
19 C. L. Johnson and A. C. Dunn, *Wear*, 2019, **438**, 203066.
20 A. Shinde, I. Siva, Y. Munde, I. Sankar, M. T. H. Sultan, F. Mustapha, F. S. Shahar and M. I. Najeeb, *J. Mater. Res. Technol.*, 2022, **21**, 1570–1580.
21 W. Huang, L. Jiang, C. Zhou and X. Wang, *Tribol. Int.*, 2012, **52**, 87–93.
22 I.-J. Chen and E. Lindner, *Langmuir*, 2007, **23**, 3118–3122.
23 E. J. Park, Y. K. Cho, D. H. Kim, M.-G. Jeong, Y. H. Kim and Y. D. Kim, *Langmuir*, 2014, **30**, 10256–10262.
24 K. Sheng, X. Dong, Z. Chen, Z. Zhou, Y. Gu and J. Huang, *Appl. Surf. Sci.*, 2022, **591**, 153097.
25 S. Kim, H. J. Hwang, H. Cho, D. Choi and W. Hwang, *Chem. Eng. J.*, 2018, **350**, 225–232.
26 T. L. Park, Y. M. Yang, D. G. Shin and D. E. Kim, *J. Korean Soc. Precis. Eng.*, 2018, **35**, 803–807.
27 G.-M. Kim, J.-W. Lee, S.-J. Lee and C.-L. Kim, *Materials*, 2022, **15**, 8736.
28 S.-J. Lee, G.-M. Kim and C.-L. Kim, *RSC Adv.*, 2023, **13**, 3541–3551.
29 S.-J. Lee, G.-M. Kim and C.-L. Kim, *Polym. Test.*, 2023, **117**, 107855.
30 C.-L. Kim and D.-E. Kim, *Sci. Rep.*, 2017, **7**, 6896.
31 D.-E. Kim, C.-L. Kim and H.-J. Kim, *CIRP Ann.*, 2011, **60**, 599–602.
32 C.-L. Kim, C.-W. Jung, Y.-J. Oh and D.-E. Kim, *NPG Asia Mater.*, 2017, **9**, e438.
33 C.-L. Kim and D.-E. Kim, *Sci. Rep.*, 2016, **6**, 20563.
34 G.-M. Kim, S.-J. Lee and C.-L. Kim, *Materials*, 2021, **14**, 4489.
35 D.-Y. Wang, C.-L. Kim and D.-E. Kim, *CIRP Ann.*, 2017, **66**, 527–530.